IEEE Access
Multidisciplinary | Rapid Review | Open Access Journal

Received January 9, 2019, accepted January 14, 2019, date of publication January 31, 2019, date of current version February 20, 2019.

Digital Object Identifier 10.1109/ACCESS.2019.2895754

Single-Carrier Spatial Modulation for the Internet of Things: Design and Performance Evaluation by Using Real Compact and Reconfigurable Antennas

D.-T. PHAN-HUY[1], (Member, IEEE), Y. KOKAR[2], K. RACHEDI[3], P. PAJUSCO[4], (Senior Member, IEEE), A. MOKH[2], T. MAGOUNAKI[1], R. MASOOD[1], C. BUEY[1], P. RATAJCZAK[1], N. MALHOUROUX-GAFFET[1], J.-M. CONRAT[1], J.-C. PRÉVOTET[2], A. OURIR[3], J. DE ROSNY[3], M. CRUSSIÈRE[2], PR. M. HÉLARD[2], (Member, IEEE), A. GATI[1], T. SARREBOURSE[1], AND M. DI RENZO[5], (Senior Member, IEEE)

[1]Orange Labs Networks, 92326 Châtillon, France
[2]INSA Rennes, CNRS, Institut d'Electronique et de Télécommunication de Rennes, UMR 6164, University of Rennes 1, 35000 Rennes, France
[3]Institut Langevin, Ecole Supérieure de Physique et de Chimie Industrielle, CNRS, 75005 Paris, France
[4]Institut Mines Telecom Atlantique, 29238 Brest, France
[5]Laboratoire des Signaux et Systèmes, CNRS, University of Paris-Saclay, CentraleSupélec, University of Paris-Sud, 91192 Gif-sur-Yvette, France

Corresponding author: D.-T. Phan-Huy (dinhthuy.phanhuy@orange.com)

This work was supported by the SpatialModulation Project under the French Research Agency under Grant ANR-15-CE25-0016.

ABSTRACT In this paper, for the first time, we propose two new solutions to boost the data rate between small connected objects such as glasses and cams and the 5th generation (5G) mobile network, based on spatial modulation, single-carrier waveform, compact reconfigurable antennas at the object side and massive multiple input multiple output (M-MIMO) at the network side. In the first new wireless communication system, a ''transmitting object'' uses transmit spatial modulation with a compact reconfigurable antenna and a constant envelop amplifier to transmit in high data rate with low complexity and low power consumption. The space-time digital processing capability of the M-MIMO 5G base station is used to detect such signal. In the second new wireless communication system, a ''receiving object'' uses receive spatial modulation, a compact multiport antenna and a low complexity detection algorithm to receive in high data rate with a low complexity signal processing. The space-time beamforming capability of the M-MIMO 5G base stations is exploited to deliver a signal that is pre-equalized enough to be detected by the object. For the first time, we present experiments showing that M-MIMO allows for the re-introduction of single-carrier modulation waveform. For the first time, we present performance results obtained with real existing compact antennas and compact reconfigurable antennas, showing that the two new communication systems outperform conventional modulation in terms of energy efficiency and complexity.

INDEX TERMS Spatial modulation (SM), receive antenna shift keying (RASK), beamforming, multiple input multiple output (MIMO), reconfigurable antennas, compact antennas.

I. INTRODUCTION

Future mobile networks of the 5th generation (5G) will provide a wireless connection to the Internet-of-Things (IoT) [1]. Among connected things, some, like connected glasses, connected cameras and connected watches, will need to transmit or receive video streams at a high data rate. The 3rd Generation Partnership Project (3GPP) has already started to lower down the cost and the power consumption of devices for connected objects by reducing the number of Radio Frequency (RF) chains (for transmission) and reducing the number of RF amplifiers [2].

Recently, it has been shown that, for some high signal to noise ratios values, and still with a single RF chain at the transmitter side, by using transmit spatial modulation [3] with conventional arrays of antenna elements [4], one can achieve

The associate editor coordinating the review of this manuscript and approving it for publication was Xianfu Lei.

a higher spectral efficiency than by using a conventional modulation with the same single RF chain [5]. In transmit spatial modulation systems, in addition to the data stream sent using a conventional Pulse shape Amplitude Modulation (PAM), an additional data stream is sent by switching the transmit antenna element, every symbol period. The index of the current transmit antenna element encodes binary information. Previous studies on transmit spatial modulation are focused on conventional arrays: [6] analyzes solutions based on spatial modulation that exploit the diversity gain of the conventional antenna array and [7]–[14] provide preliminary results on the performance of transmit spatial modulation based on experimental data obtained with conventional antenna arrays. Studies on optimal and low-complexity receiver designs are available as well, e.g., [15]–[17]. For more information on transmit spatial modulation, please refer to the survey papers [18]–[22]. In addition, spatial modulation is a special case of index modulation [21], and other related technologies are media-based modulation [23], space-time channel modulation [24], and quadrature channel modulation [25]. Further recent options can be found in [21]. In receive spatial modulation systems such as the ones studied in [26], in addition to sending a conventional PAM, the transmitter sends an additional data stream by focusing towards one antenna of the receiver among several, every symbol period. The index of the target antenna encodes binary information. A simple receiver can be used to demodulate the two streams [27]–[29].

Other works on reconfigurable antennas [30]–[32] suggest that one can transport more bits than with a SISO system by using a reconfigurable antenna. In this case, instead of switching between antenna elements, the transmitter switches between radiation patterns. The advantage of these solutions is that they are more compact in size. The limitation of these techniques is the non-orthogonality of the radiation patterns, and up to now, no complete performance study with real and existing compact antennas has been performed to verify the advantage of such antennas.

In parallel, 5G envisions the development of massive arrays [34]–[36] at the network side, with hundreds of antenna elements. These Massive Multiple Input Multiple Output (M-MIMO) antennas benefit from higher beamforming and spatial multiplexing gains [34], [35], or reduced complexity in the demodulation [36].

In this paper, for the first time, we introduce and make a complete performance evaluation of two new communication systems illustrated in Figure 1, for uplink and downlink communications, respectively, between objects with compact antennas and a base station with M-MIMO antenna array. In the uplink, transmit spatial modulation is used, and the object antenna is a compact reconfigurable antenna (either a multiport switchable antenna or a monoport reconfigurable antenna), whereas in the downlink, receive spatial modulation is used and the object antenna is still a compact antenna but multiport only in the current implementation. These two original and new systems are compared to systems using conventional modulation schemes as well.

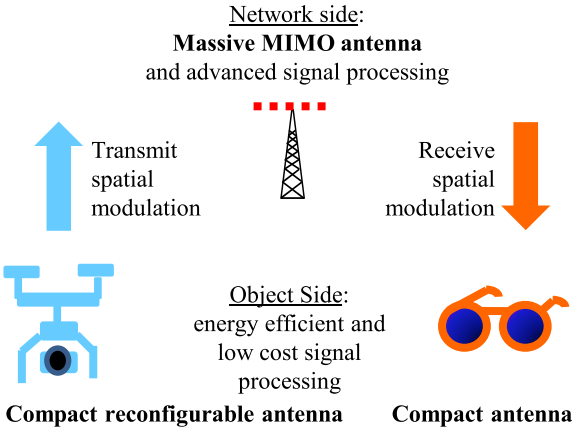

FIGURE 1. Connecting objects to the network thanks to transmit spatial modulation, receive spatial modulation, compact antennas, compact reconfigurable antennas and massive MIMO antennas.

The paper is organized as follows: Section II recalls transmit spatial modulation and receive spatial modulation concepts and illustrates these concepts with visual experiments. Section III and IV present the performance evaluation study for transmit spatial modulation and receive spatial modulation, respectively.

The following notation is used throughout the paper. If $x \in \mathbb{C}$, then $|x|$ is its module, $\arg(x)$ is its phase in radians, x^* is its conjugate, $\mathcal{R}e(x)$ is its real part and $\mathrm{Im}(x)$ is its imaginary part. If $\in \mathbb{C}^{M\times P}$, then $\mathbf{H}^\dagger$ is the transpose-conjugate of $\mathbf{H}$ and $\|\mathbf{H}\|^2 = \sum_{p=0}^{P-1}\sum_{m=0}^{M-1}\left|\mathbf{H}_{m,p}\right|^2$. If $\mathbf{x} \in \mathbb{C}^{P\times 1}$, then $\|\mathbf{x}\|^2 = \sum_{p=0}^{P-1}\left|\mathbf{x}_p\right|^2$. $[n, p]$ is the set of integers between n and p, including n and p. $\mathrm{j}^2 = -1$. We define the set $\mathcal{B}^{(P)}$, S^{QPSK}, S^{8PSK} and S^{16QAM} as follows:

- $\mathcal{B}^{(P)} = \{\mathbf{b}^{(l)} \in \{0,1\}^{K\times 1} | l \in [1, P]; K = \log_2(P); \sum_{k=1}^{K}\mathbf{b}_k^{(l)}2^{k-1} = l\}$;
- $S^{QPSK} = \{\frac{1+\mathrm{j}}{\sqrt{2}}, \frac{1-\mathrm{j}}{\sqrt{2}}, \frac{-1-\mathrm{j}}{\sqrt{2}}, \frac{-1+\mathrm{j}}{\sqrt{2}}\}$;
- $S^{8PSK} = \left\{e^{\frac{2\mathrm{j}\pi(n-1)}{8}}, \mathrm{n} \in [\![1; 8]\!]\right\}$;
- $S^{16QAM} = \left\{\frac{-3+2l+(-3+2k)}{\sqrt{10}} l \in [0, 3] \text{ and } k \in [0, 3]\right\}$.

II. TRANSMIT SPATIAL MODULATION AND RECEIVE SPATIAL MODULATION CONCEPTS

A. TRANSMIT SPATIAL MODULATION

In this section, we recall the concept of transmit spatial modulation and illustrate this concept with a visual experiment illustrated in Figure 2.

During the communication, the transmitter activates one radiation pattern among $P = 2^K$ distinct ones. Each radiation pattern is associated with a distinct binary sequence of K bits, according to a pre-defined pattern-to-bit mapping rule. The rule is known at both the transmitter and the receiver sides. As in most wireless communication systems, the transmitter sends pilots to train the receiver. More precisely, the transmitter activates each of its radiation patterns alternatively, so that the receiver can estimate and store the propagation channel

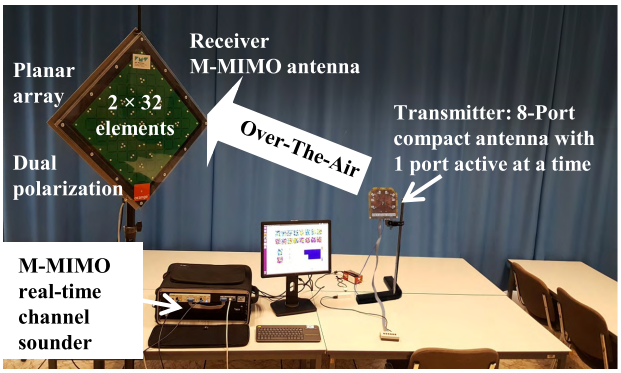

FIGURE 2. Experimental set-up.

associated with each pattern. Then, the transmitter performs an actual data transmission as follows. A long binary sequence is cut into sub-sequences of K bits. To transmit a particular sub-sequence, the transmitter activates the pattern that corresponds to the sub-sequence, using the pattern-to-bit mapping rule. The receiver detects the pattern that has been used by comparing the current received channel with the P stored channels. The receiver converts the detected pattern into a sub-sequence of K bits using the pattern-to-bit mapping rule. Note that, transmit spatial modulation can be combined with a conventional modulation.

As illustrated in Figure 2, our visual experiment involves an 8-port compact antenna at the transmission side and a 64-element M-MIMO antenna at the receiver side. The transmitter emits a signal with carrier frequency of 2.45 GHz with one antenna port among the $P = 8$ available, thanks to a switch. In this case, a pattern encodes $K = 3$ bits. As illustrated in Figure 3, the 8 radiation patterns corresponding to the 8 ports of this antenna are distinct. Figure 3 also provides the mapping rule between patterns and 3-bit sequences.

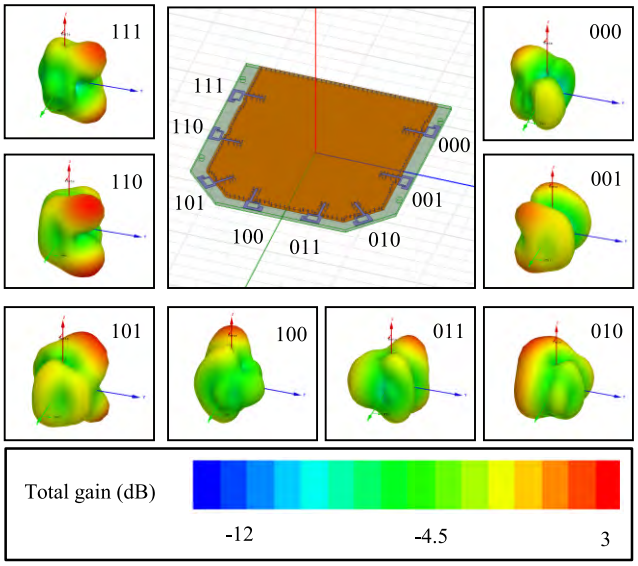

FIGURE 3. The 8 ports of the transmitter, their corresponding radiation patterns and their corresponding 3-bit sequences.

As illustrated in Figure 2, the 64 elements of the M-MIMO antenna are positioned on a grid of 8 lines and 8 columns and connected to a real-time channel sounder. Figure 4 illustrates the graphical interface of the sounder. The top of Figure 4 illustrates the result of a previous channel training phase. For each of the 8 radiation patterns, the spatial signature (i.e., the matrix of 8 by 8 estimated channel amplitudes) is stored and displayed in color scale. Each spatial signature is associated with a pattern and a 3-bit sequence. The bottom of Figure 4 illustrates the data transmission. A 3-bit sequence is transmitted by activating one radiation pattern among the 8 available. The channel sounder displays the current spatial signature (i.e., the actual 8 by 8 matrix of amplitudes of the current channel) in a color scale, computes the correlation of this matrix with the 8 stored matrices, determines the pattern that maximizes the correlation, and converts it into the detected 3-bit sequence, using the pattern-to-bit mapping rule. As illustrated in a video [38], all these steps are done in real time. In [38], even though the channel training is done only once at the beginning of the video, the detection remains robust for a long time period. This is thanks to the large size of the 8 by 8 matrices on which the correlation is performed. This illustrates one of the advantages of using M-MIMO at the network side.

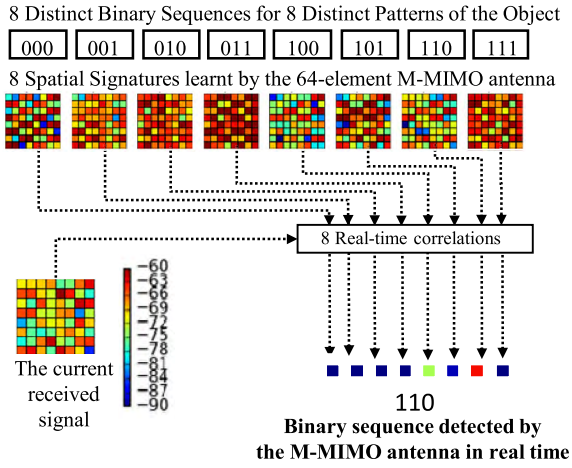

FIGURE 4. Graphical interface of the M-MIMO real time channel sounder.

Note that the training phase of spatial modulation is equivalent to the channel estimation phase for a conventional single-carrier modulation. Both modulations require the transmission of pilot symbols during these phases, with the same periodicity (enough to track the channel variation).

B. RECEIVE SPATIAL MODULATION

In this section, we recall the concept of receive spatial modulation and illustrate this concept with a visual experiment depicted in Figure 5.

The receiver has $P = 2^K$ antenna ports with P distinct associated radiation patterns. Each radiation pattern is associated with a distinct binary sequence of K bits, according to a pre-defined pattern-to-bit mapping rule. The rule is

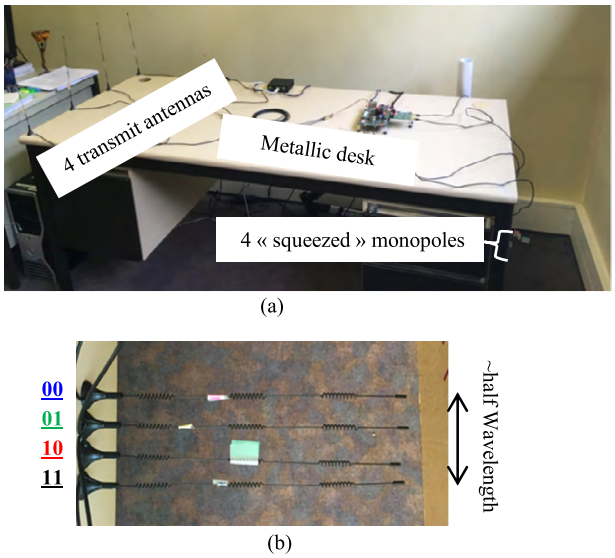

FIGURE 5. Experimental set-up. (a) Experimental set-up, non line-of-sight (NLOS). (b) Zoom on the 4 ≪ squeezed ≫ monopoles.

known at both the transmitter and the receiver sides. Channel reciprocity based beamforming (BF) as implemented in time division duplex (TDD) mode systems is used in order to target one antenna of the receiver among P. As in any channel reciprocity based BF system, during the training phase the receiver sends distinct pilots from its distinct ports so that, for each port, the transmitter can: 1) estimate the channel, and 2) compute and store the precoder that enables to beamform towards this particular port. Then, the transmitter performs data transmission as follows. A long binary sequence is cut into sub-sequences of K bits. To transmit a particular sub-sequence, the transmitter uses the stored precoder that beamforms towards the pattern corresponding to the considered sub-sequence. Finally, after detecting the port that is the current target of the beamforming (for instance by identifying the port that receives the strongest power), the receiver converts the detected pattern into a sub-sequence of K bits using the pattern-to-bit mapping rule. Note that, this can be combined with a conventional modulation.

In our visual experiment, a transceiver and a receiver detailed in [39] are used with a carrier frequency of 2.48 GHz.

As illustrated in Figure 5, the transmitter is a uniform linear array (ULA) of 4 monopoles and the receiver is a ULA of $P = 4$ "squeezed monopoles". These monopoles are "squeezed" in the sense that they are close to each other by much less than half a wavelength and subject to coupling. In this experiment, the transmitter uses maximum ratio transmission (MRT) beamforming [40], and switches at a maximum speed of 125 kHz between the four different stored precoders, each precoder targeting a distinct "squeezed monopole". In this example, the identity of the target "squeezed monopole" encodes $K = \log_2(P) = 2$ bits. In parallel, the system transmits BPSK symbols.

Figure 6 illustrates the resulting constellation of receive spatial modulation together with BPSK modulation. The positions of the two BPSK states in the complex I-Q domain are visualized by two drawings of targets. The I-Q symbol received by each of the $P = 4$ monopoles of the receiver is plot for different realizations of the propagation channel. The joint detection of BPSK and the spatial modulation consists in determining the monopole that is closest to one of the two BSPK states. Figure 6 illustrates experimental measurements of the received I-Q symbols. The measurements are classified into 8 different categories illustrated by 8 different

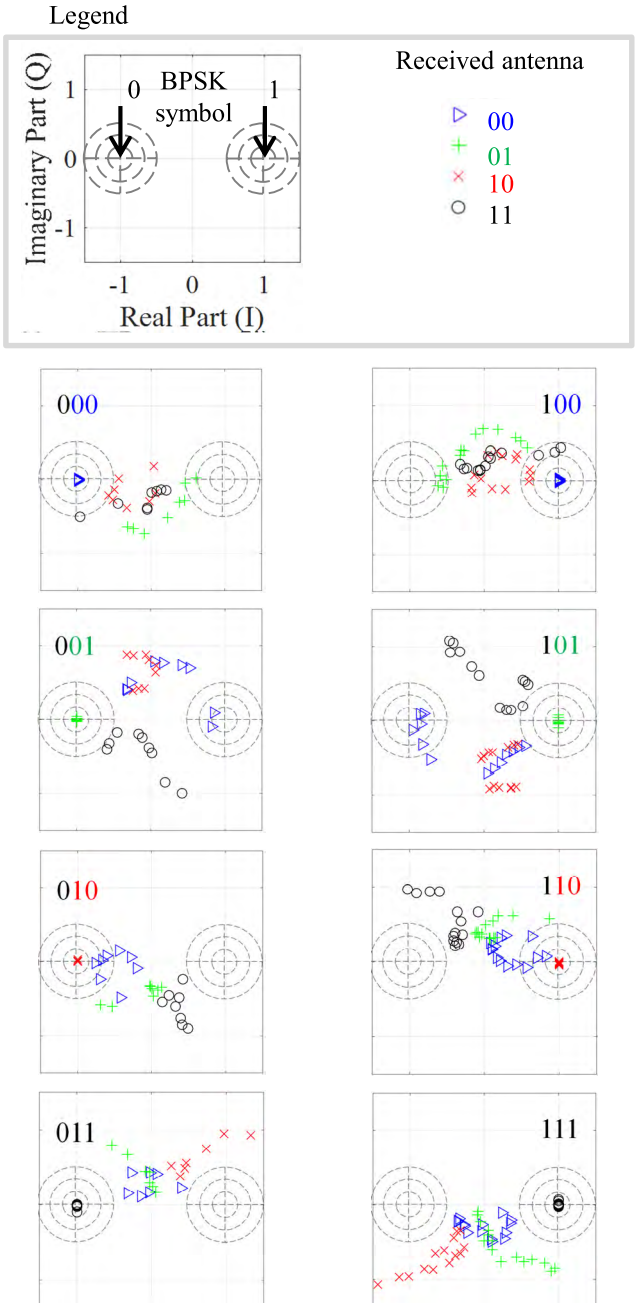

FIGURE 6. Experimental observations of the constellations for receive spatial modulation and BPSK modulation.

figures. For each category, the same BPSK symbol and the same spatial modulation symbol are detected. One can note that spatial modulation works even with these ''squeezed monopoles''. This is due to the fact that for one monopole the other monopoles act as parasitic scatterers. This phenomenon is known to create decorrelation and is exploited as a design principle for the compact multiport antennas presented in [41] and [42]. These same antennas are actually the ones used in the studies described in Sections IV and V.

III. MASSIVE MIMO: AN ENABLER FOR SINGLE-CARRIER MODULATIONS

5G is based on multi-carrier modulation. Such modulation is not compatible with spatial modulation [20]. However, we believe that the introduction of M-MIMO antennas in 5G networks is an enabler for the re-introduction of single-carrier modulation in the future. In previous works [43], [44], it has been shown that thanks to time reversal focusing with a large number of transmit antennas, the signal at the receiver is nearly echo-free. In [44], a single-tap receiver successfully demodulates a signal using a single-carrier modulation, within a 30MHz bandwidth centered at 1 GHz and using a 256 Quadrature Amplitude Modulation (QAM). However, this experiment was performed using an arbitrary waveform generator at the transmission side, and an oscilloscope at the reception side.

In this paper, we show recent experimental results obtained using the open-source hardware and software development platform Open Air Interface (OAI), and a rail moving with a Digital Servo Amplifier, SERVOSTAR 300, along with a Rosier servo motor controlling the movement. OAI is a wireless technology platform that offers an open-source software-based implementation of the Long Term Evolution (LTE) system spanning the full protocol stack of 3rd Generation Partnership Project (3GPP) standard both in Evolved Universal Terrestrial Radio Access Network (E-UTRAN) and Evolved Packet Core (EPC). The experiments were carried out using orthogonal frequency division multiplex (OFDM) frames at the carrier frequency of 2.68 GHz. Each OFDM symbol consists of 512 carriers, out of which 300 are filled with random QPSK symbols and the rest are set to zero. An extended cyclic prefix (ECP) of 128 samples is added to each OFDM symbol after the 512-point Inverse Fast Fourier Transform (IFFT). The sampling rate is 7.68 mega symbols per second, resulting in an effective bandwidth of 4.5 MHz. Ten sub-frames, each with 12 ECP-OFDM symbols, compose the TDD OFDM frame.

In the experiment, the receiver sends pilots called sounding reference signals (SRS) in the uplink direction. The transmitter uses these pilots to estimate the uplink channel. Channel reciprocity is exploited to deduce the downlink channel. The transmitter precodes its downlink data and pilots with a maximum ratio transmission (MRT) precoder, to beamform the signal towards the receiver. Note that MRT is equivalent to time reversal or to transmit matched filter pre-filtering (applied to OFDM instead of a single-carrier modulation) [39]. During the experiment, 15 different positions of the receiver are tested, along a rail, and all in NLOS of the transmitter. For each position, the receiver measures the frequency response of the received beamformed channel thanks to the downlink precoded pilots. The measurements were carried out inside a controlled laboratory environment. Figure 7 illustrates the measurement setup.

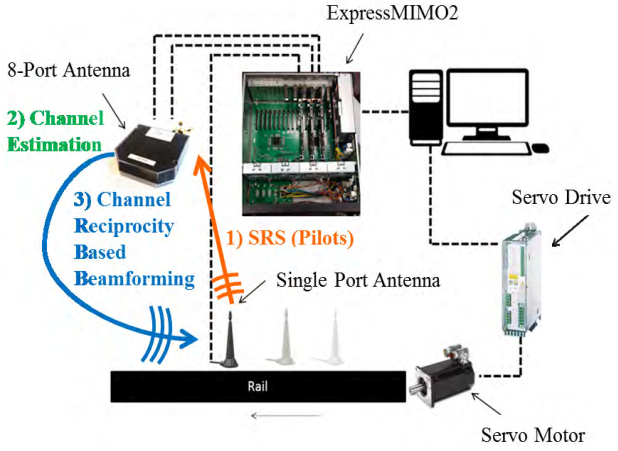

FIGURE 7. Experimental set-up, in NLOS.

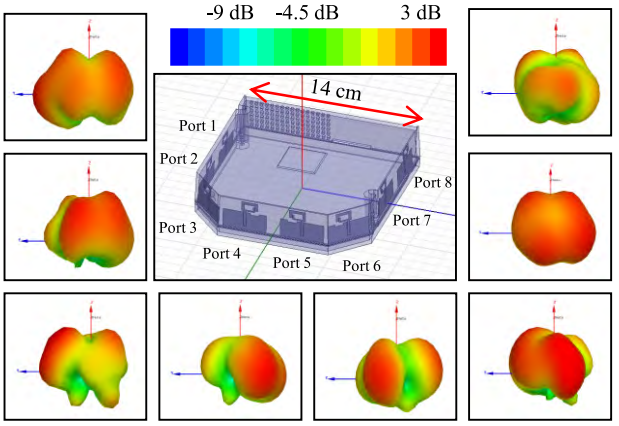

FIGURE 8. 8-port transmit antenna.

Figure 8 illustrates the radiation patterns of the 8 ports of the transmitter. Although, the antenna is compact, it exhibits patterns that are diverse. This antenna is therefore equivalent to an array of 8 low-correlated antennas.

Figure 9 illustrates the propagation environment during the experiments. Non-line-of sight propagation is chosen to create multi-path propagation. In such environment, the channel impulse response has several delayed taps. Hence, a single-tap receiver trying to demodulate a single-carrier modulation would suffer from inter-symbol interference. Finally, we apply an IFFT to the frequency response of the received beamformed channel, to obtain the corresponding filter in the time domain.

Figure 10 illustrates the measured frequency response and the corresponding impulse response, for the received

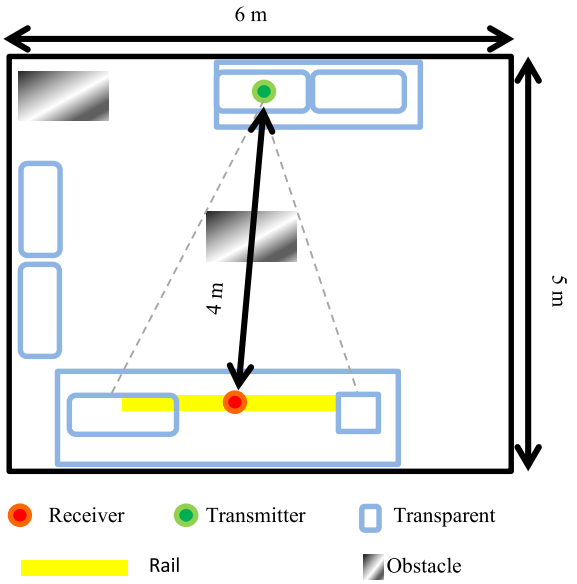

FIGURE 9. NLOS propagation.

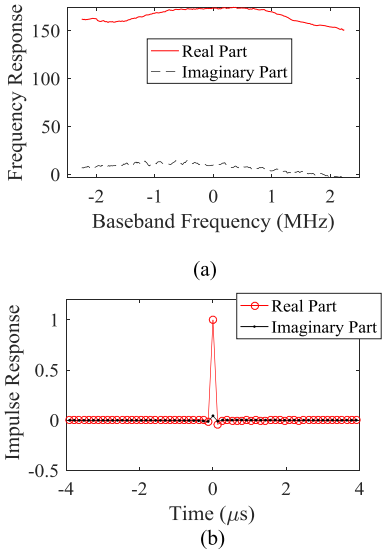

FIGURE 10. Received beamformed channel for the 15th position of the UE. (a) Frequency response. (b) Impulse response.

beamformed channel measured at the 15th position. We observe that the beamformed channel is nearly a single-tap channel. We also evaluate the ratio between the useful signal and the inter-symbol interference (SIR) that would be undergone by a single-tap receiver demodulating a single-carrier modulation at 5 MHz. As illustrated in Figure 11, for all tested positions, this value exceeds 20 dB. This is largely sufficient to support a single-carrier modulation with 16 QAM. More precisely, for the worst case position (position number 3), we simulate the transmission of 1,500,000 random bits over a single-carrier modulation transmission with a Raised Root Cosine (RRC) filter, 16 QAM, and a single-tap receiver. For this simulation we chose an extreme value

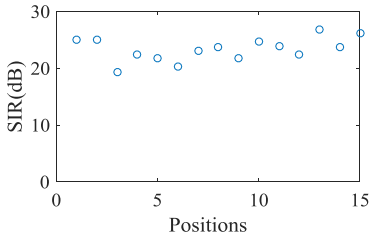

FIGURE 11. SIR with single-carrier modulation.

of Roll Off factor (0.001), to test the worst case scenario. We use the same simulation methodology detailed in [44], except that we use the current measured beamformed channel impulse response. The resulting measured bit error rate over 1,500,000 bits is zero. This means that the attainable BER, in this case, is estimated to be lower than 10^{-5}.

This confirms that current standards for mobile networks have the potential to support single-carrier modulations, with bandwidths as large as several MHz. Note that, by applying maximum ratio combining (MRC) at the receiver side (instead of MRT at the transmitter side), in an uplink transmission (instead of a downlink transmission) we would have obtained the same result: the channel after equalization would have been single-tap. This means that after a receive matched filter, the channel is single-tap and compatible with a single-carrier modulation and a single-tap detector.

In the next sections, M-MIMO is used with much more antenna elements than in the current sub-section. It is therefore a reasonable assumption to consider that the beamformed or equalized channel (using transmit matched filtering or received matched filtering) will be single-tap, i.e., not frequency selective. As a consequence, to derive the beamformed channel, one just needs to study the frequency-flat channel over the carrier frequency. Therefore, in the next sections, we will directly use a frequency-flat channel model for our performance studies and assume that the equalized or pre-equalized channel does not introduce interference between successive symbols in the time domain.

IV. UPLINK TRANSMISSION: FIRST PERFORMANCE EVALUATION OF TRANSMIT SPATIAL MODULATION WITH REAL COMPACT RECONFIGURABLE ANTENNAS

In this section, for the first time, we present a complete performance evaluation of a wireless communication system using transmit spatial modulation with a real and existing compact reconfigurable antenna at the transmitter side and an M-MIMO antenna at the receiver side. The considered carrier frequency in this section is 2.45 GHz.

A. MODELS OF REAL COMPACT RECONFIGURABLE ANTENNAS AND THE PROPAGATION CHANNEL

At the base station side, we consider a ULA of $M = 64$ elements spaced by half a wavelength as an example of M-MIMO antenna.

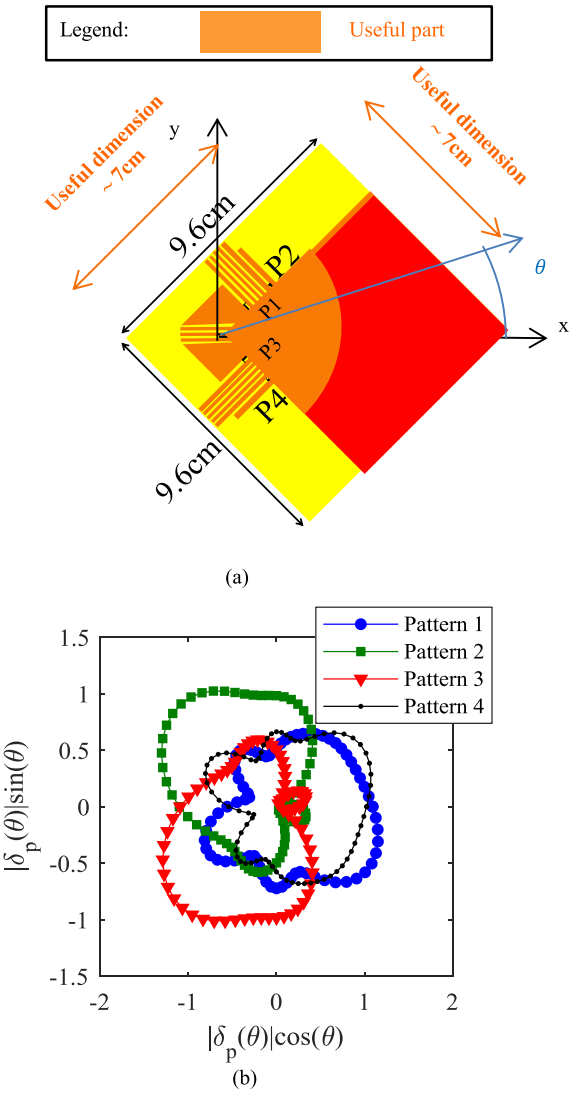

FIGURE 12. Compact multiport switchable antenna model. (a) Antenna dimensions and convention for θ. (b) 2-D radiation patterns, where θ is the angle of arrival or departure and $\delta_p(\theta)$ is the antenna gain in the direction of θ for port p.

As for the object, two different real and existing compact reconfigurable antennas are considered and compared:

- A multiport switchable antenna [42] illustrated in Figure 12-a) that can generate $P = 4$ different radiation patterns, and that can therefore transmit $K = \log_2(P) = 2$ bits by using spatial modulation;
- A monoport reconfigurable antenna [46] illustrated in Figure 13-a) that can generate $P = 2$ different radiation patterns, and that can therefore transmit $K = \log_2(P) = 1$ bit by using spatial modulation.

The first one is half of the wavelength in size, whereas the second one only occupies one third. For both antennas, only one radiation pattern is activated at a time, either thanks to a RF switch connected to the multiport antenna or by commuting the diodes of the reconfigurable antenna [46].

The two-dimensional (2D) propagation models, for the multiport switchable antenna and the monoport reconfigurable antenna are illustrated in Figure 14 and Figure 15, respectively. For the two compact reconfigurable antennas, the complex gain function $\delta_p(\theta)$ ($\delta_p : R \longrightarrow C$) of each pattern p in direction angle θ is numerically characterized by using Finite Difference Time Domain (FDTD) full wave simulation. The moduli of the radiation patterns are illustrated in Figure 12-b) and Figure 13-b), for the multiport switchable antenna and the monoport reconfigurable antenna, respectively.

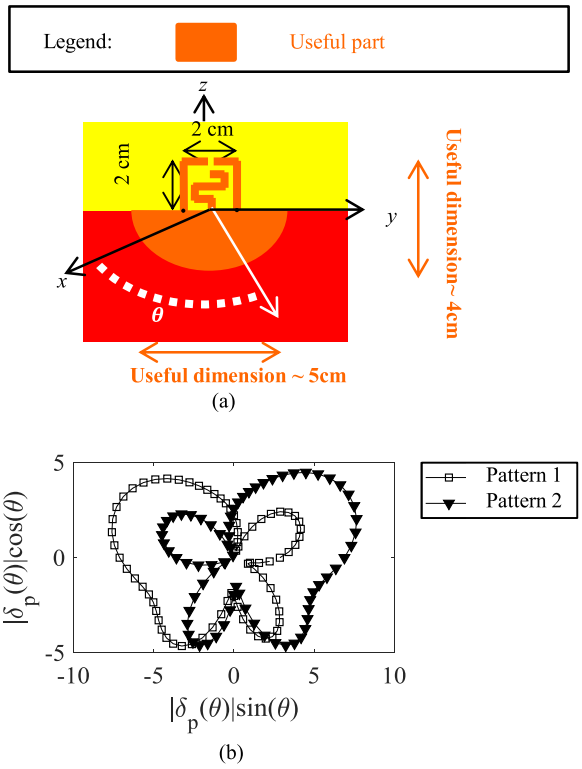

FIGURE 13. Compact monoport reconfigurable antenna model. (a) Antenna dimensions and convention for θ. (b) 2-D radiation patterns, where θ is the angle of arrival or departure and $\delta_p(\theta)$ is the antenna gain in the direction of θ for radiation pattern p.

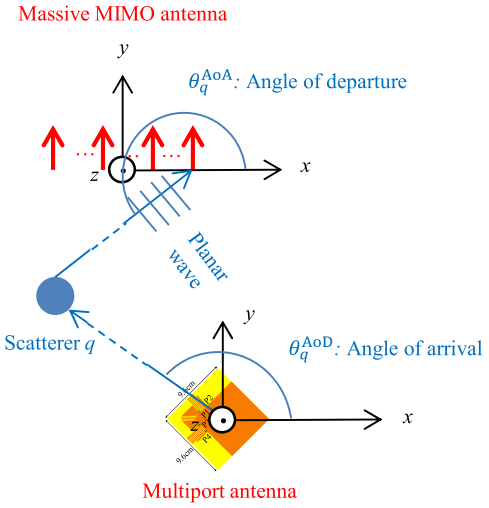

FIGURE 14. Propagation model for the multiport switchable antenna.

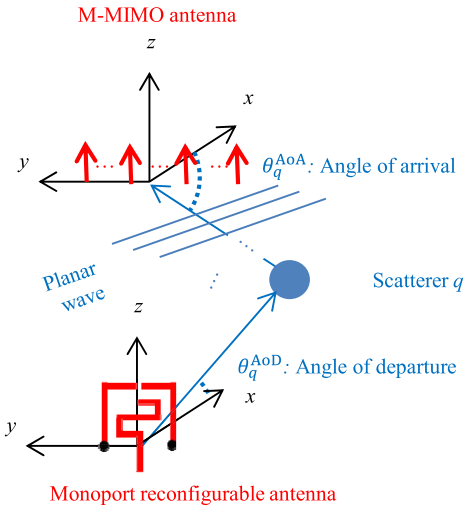

FIGURE 15. Propagation model for the monoport reconfigurable antenna.

The spatial correlation between two radiation patterns p and q of the same antenna is a key parameter in spatial modulation systems. The less correlated the patterns are, the more robust spatial modulation to noise is. The correlation is given by:

$$\psi^{p,q} = \frac{\left|\int_{\theta=0}^{2\pi} \delta_p(\theta)\,\delta_q^*(\theta)\,d\theta\right|^2}{\left(\int_{\theta=0}^{2\pi} |\delta_p(\theta)|^2\,d\theta\right) \times \left(\int_{\theta=0}^{2\pi} |\delta_q(\theta)|^2\,d\theta\right)}$$

Table 1 and Table 2 provide the discrete correlations for the multiport switchable antenna and the monoport reconfigurable antenna, respectively. These correlations are computed based on the discrete values of the δ_p functions obtained by FDTD simulations

TABLE 1. Correlations $\psi^{p,q}$ between antenna ports p and q for The multiport switchable antenna.

p\q	1	2	3	4
1	1	0.0722	0.0593	0.0007
2	0.0772	1	0.0158	0.0522
3	0.0593	0.0158	1	0.0688
4	0.007	0.0522	0.0688	1

TABLE 2. Correlations $\psi^{p,q}$ between antenna ports p and q for the monoport reconfigurable antenna.

p\q	1	2
1	1	0.3190
2	0.3190	1

We consider a single-carrier modulation communication. As explained in section III, thanks to the M-MIMO antenna and assuming that a matched filter is used at the receiver, we can limit the study to a frequency-flat channel and assume that the channel does not introduce interference between successive symbols in the time domain. The wireless propagation channel between one antenna port of the transmitter and one antenna element of the receiver can be modeled by a complex gain.

We define $\mathbf{H} \in \mathbb{C}^{M\times P}$ as the channel between the object and the base station. More precisely, let $\mathbf{H}_{m,p}$ be the channel coefficient between the receive antenna $m \in [1, M]$ of the base station and the object when it is using the radiation pattern number $p \in [1, P]$. $\mathbf{H}_{m,p}$ includes both the wireless propagation and the radiation pattern p.

Regarding the model used for multi-path propagation, we consider a 2D wireless propagation model, with Q random scatterers creating angular diversity in the channel. The elements of the M-MIMO antenna are spatially correlated. The path $q \in [1, Q]$ between the receive antenna m of the base station and the connected object has a random complex gain $\Gamma_q \in \mathbb{C}$, a random angle of departure $\theta_q^{\text{AoD}} \in [0, 2\pi[$ and a random angle of arrival $\theta_q^{\text{AoA}} \in [0, 2\pi[$. Γ_q is a Rayleigh fader with $E\left[\left|\Gamma_q\right|^2\right] = 1/\text{Q}$ and θ_q^{AoD} and θ_q^{AoA} are uniformly distributed over $[0, 2\pi[$. With these notations, the channel coefficient $\mathbf{H}_{m,p}$ is given by:

$$\mathbf{H}_{m,p} = \rho \sum_{q=1}^{Q} \Gamma_q \delta_p\left(\theta_q^{\text{AoD}}\right) e^{j\pi.sin\left(\theta_q^{\text{AoA}}\right)(m-1)}, \quad (1)$$

where ρ is a normalizing factor. We choose ρ such that:

$$\frac{\|\mathbf{H}\|^2}{PM} = 1.$$

In other terms, the average channel power per SISO antenna link is unitary.

B. SYSTEM MODEL

For the compact multiport switchable antenna, we compare five different schemes to send a sequence $\mathbf{b}$ of r bits, where, $\mathbf{b} = \mathbf{b}_1 \ldots \mathbf{b}_r \in \mathcal{B}^{(\mathbf{r^2})}$, and $r = 4$:

- "16QAM & Pattern $p = 1$";
- "16QAM & Pattern $p = 2$";
- "16QAM & Pattern $p = 3$";
- "16QAM & Pattern $p = 4$";
- "QPSK & SM4".

For the compact monoport reconfigurable antenna, we compare three different schemes to send a sequence $\mathbf{b}$ of r bits, where $\mathbf{b} = \mathbf{b}_1 \ldots \mathbf{b}_r \in \mathcal{B}^{(\mathbf{r^2})}$, with $r = 4$:

- "8PSK & Pattern $p = 1$";
- "8PSK & Pattern $p = 2$";
- "QPSK & SM2".

For all schemes, for each symbol period, the object sends a sequence of r bits $\mathbf{b} \in \mathcal{B}^{(\mathbf{r^2})}$ with a radiation pattern p. Among these $r > 0$ bits, $u > 0$ bits are sent using a complex modulation symbol $s \in S$, where S is the pre-defined set of complex modulation symbols. $K \geq 0$ bits are sent using spatial modulation. So, the following holds:

$$r = u + K.$$

The definition of S, the values of p, u and K are scheme-specific and provided in Table 3 and Table 4 for the schemes with the multiport switchable antenna and the monoport reconfigurable antenna, respectively. Note that, for "16QAM & Pattern p" and "8PSK & Pattern p", the radiation pattern p is fixed, and spatial modulation is unused ($K = 0$). On the contrary, for "QPSK & SM4" and "QPSK & SM2" schemes, the pattern p is variable and spatial modulation is used ($K > 0$).

TABLE 3. Spectral efficiency r for the compact multiport switchable antenna (with P = 4 states), in number of bits per symbol period.

Scheme	p	S	$u+K=r$
16 QAM with Pattern 1	1	S^{16QAM}	4 + 0 = 4
16 QAM with Pattern 2	2		
16 QAM with Pattern 3	3		
16 QAM with Pattern 4	4		
QPSM & SM4	1 to 4	S^{QPSK}	2 + 2 = 4

TABLE 4. Spectral efficiency r for the compact monoport reconfigurable antenna (with P = 2 states), in number of bits per symbol period.

Scheme	p	S	$u+K=r$
16 QAM with Pattern 1	1	S^{16QAM}	4 + 0 = 4
16 QAM with Pattern 2	2		
16 QAM with Pattern 3	3		
16 QAM with Pattern 4	4		
QPSM & SM4	1 to 4	S^{QPSK}	2 + 2 = 4

More precisely, in the "QPSK & SM4" scheme, as illustrated in Figure 16, during each symbol period, $\mathbf{b}_1\mathbf{b}_2$ is sent using QPSK. Simultaneously, $\mathbf{b}_3\mathbf{b}_4$ is sent using the corresponding pattern number p (based on Table 5).

TABLE 5. Pattern-to-bit mapping rule.

$\mathbf{b}_3\mathbf{b}_4$	00	10	01	11
p	1	2	3	4

In the "QPSK & SM2" scheme, as illustrated in Figure 17, during each symbol period, $\mathbf{b}_1\mathbf{b}_2$ is sent using QPSK modulation. Simultaneously, $\mathbf{b}_3$ is sent using the corresponding pattern number p (pattern $p = 1$ corresponding to Bit "0" and $p = 2$ corresponding to Bit "1").

Figure 18 and Figure 19 illustrate the mapping between bits and symbols for the schemes with the multiport antenna and the reconfigurable antenna, respectively. Note that with the chosen definitions, $E\left[|s|^2\right] = 1$ for all schemes. In other terms, all schemes radiate the same transmit power per symbol, on average.

For any scheme, we define X as follows:

$$X = \{\mathbf{x}^{(l)} \in \{0, 1\}^{P\times 1} \,|1 \le l \le r, \quad \mathbf{x}_l^{(l)} = 1 \;\&\; \mathbf{x}_{p\neq l}^{(l)} = 0.$$

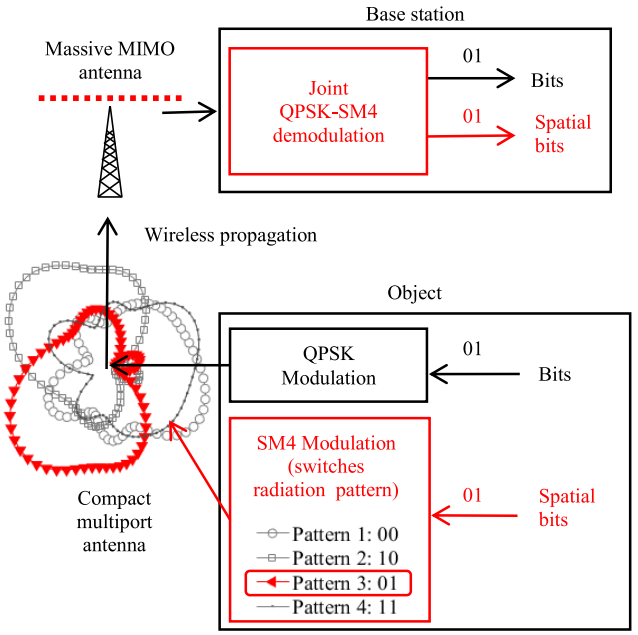

FIGURE 16. "QPSK & SM2" system model for the multiport compact antenna.

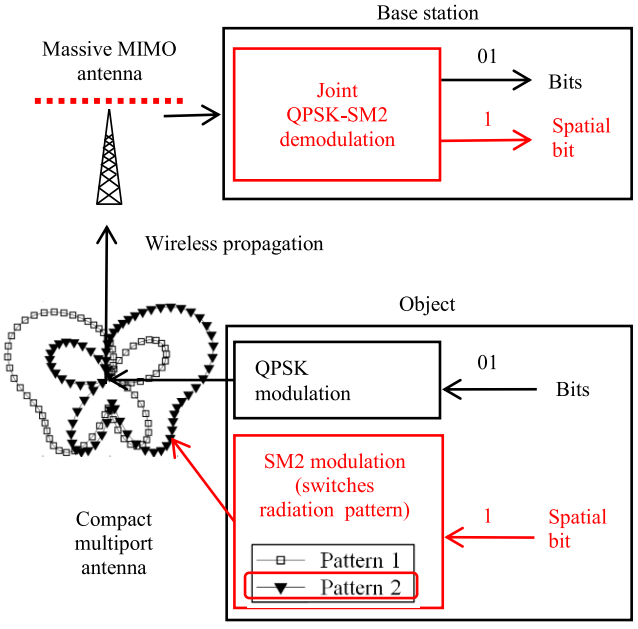

FIGURE 17. "QPSK & SM2" system model for the monoport compact antenna.

Let $\mathbf{y} \in C^{M\times 1}$ be the signal received over the M elements of the M-MIMO antenna, $\mathbf{y}$ is given by:

$$\mathbf{y} = \mathbf{\Gamma}\left(\mathbf{H}\mathbf{x}s\sqrt{P_u} + \boldsymbol{\nu}\right),$$

where $\mathbf{x} \in X$, $s \in S$, P_U is the transmit power, $\boldsymbol{\nu} \in \mathbb{C}^{M\times 1}$ is the vector of noise samples over the M receiver chains of the base station, and $\mathbf{\Gamma} \in \mathbb{C}^{P\times M}$ accounts for the

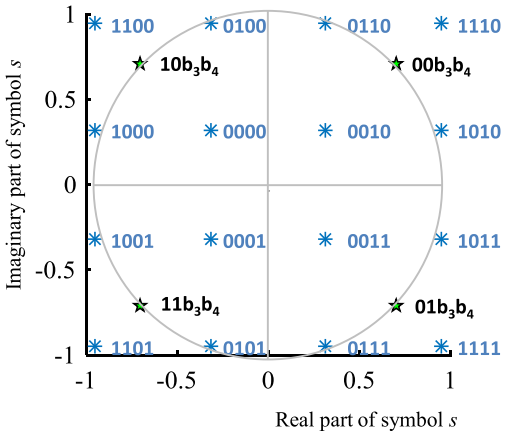

Legend

Position of s in the complex plan	Value of b	Scheme
✳	$b_1b_2b_3b_4$	16QAM
★	$b_1b_2b_3b_4$	QPSK & SM4

FIGURE 18. Constellations for 16QAM, "QPSK & SM4", with same average radiated power.

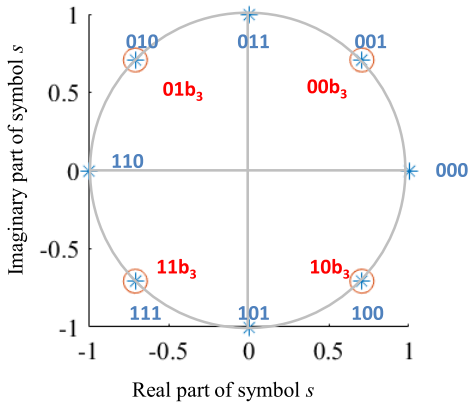

Position of s in the complex plan	Value of b	Scheme
✳	$b_1b_2b_3$	8PSK
○	$b_1b_2b_3$	QPSK & SM2

FIGURE 19. Constellations for 8PSK, "QPSK & SM2", with same average radiated power.

MRC receiver. More precisely, for $1 \leq p \leq P$ and $1 \leq n \leq M$, $\mathbf{\Gamma}_{p,n}$ is given by:

$$\mathbf{\Gamma}_{p,n} = \frac{\mathbf{H}^*_{n,p}}{\sum_{m=1}^{M} \left|\mathbf{H}_{p,m}\right|^2}.$$

We denote $P_{\text{NOISE}} = \frac{E\left[\|\boldsymbol{\nu}\|^2\right]}{M}$, as the average receiver noise power per antenna element at the base station side. We define an arbitrary signal to noise ratio metric *SNR* that is common to all schemes:

$$SNR = \frac{P_{\text{U}}}{P_{\text{NOISE}}}.$$

We also assume that the receiver has a perfect estimate of $\mathbf{H}$ thanks to a previous training phase based on pilots. We assume that the receiver has computed and stored the following set of variables:

$$Y^{ref} = \left\{ y = \mathbf{\Gamma H x} s\sqrt{P_u} | \mathbf{x} \in X \ \& \ s \in S \right\}.$$

Upon the reception of a new signal $\mathbf{y}$, the receiver compares it to the variables of Y^{ref} and determines the signal $\hat{\mathbf{y}}$ that minimizes the Mean Square Error:

$$\hat{\mathbf{y}} = \left\{ \frac{\|z - y\|^2}{M} | z \in Y^{ref} \right\}.$$

Then, the detected binary sequence $\hat{\mathbf{b}} = \hat{\mathbf{b}}_1 \ldots \hat{\mathbf{b}}_r$ is deduced from $\hat{\mathbf{y}}$ by using the mapping rules illustrated in Figure 18 and Figure 19. The bit-error-rate (BER) can then be computed as follows:

$$BER = \frac{\sum_{k=1}^{r} \left|\hat{\mathbf{b}}_k - \mathbf{b}_k\right|}{r}.$$

We perform 250,000 simulation runs. For each simulation run:

- The parameter *SNR* and the number of scatterers $Q = 10$ are fixed.
- We compute a random channel sample $\mathbf{H}$ based on randomly and independently generated parameters Γ_q, θ_q^{AoD}, θ_q^{AoA}, $\varphi_{m,q}^{\text{AoD}}$, $\Lambda_{m,q}$ and $\boldsymbol{\nu}$.
- We generate a random sample of noise $\boldsymbol{\nu}$.
- For each possible values of the sent sequence $\mathbf{b}$, i.e. for all $\mathbf{b} \in B^{(16)}$, we compute $\mathbf{y}$, $\hat{\mathbf{y}}$ and $\hat{\mathbf{b}}$ and the BER.

We average these BER values over all sent sequences, during a simulation run, and over all runs (i.e. over 1 million of bits). We then plot the result as a function of *SNR* in Figure 20 and Figure 21, for the multiport antenna, and the monoport reconfigurable antenna, respectively.

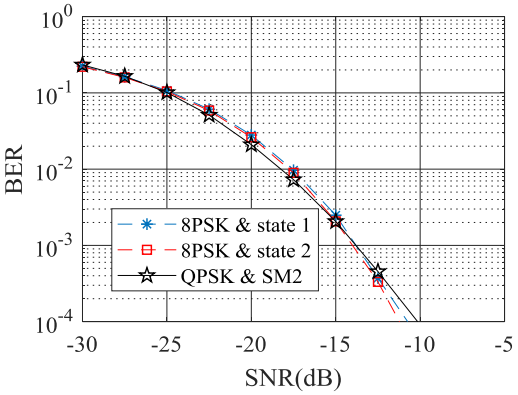

FIGURE 20. Performance with the monoport reconfigurable Antenna.

C. SIMULATION RESULTS AND CONCLUSIONS

Figure 20 shows that the compact monoport reconfigurable antenna with "QPSK & SM2" modulation is a solution to provide 3 bits/s/Hz, that is as efficient and as compact in

size as another solution using a compact antenna of the same size with a conventional 8PSK modulation. However, the monoport reconfigurable antenna with "QPSK & SM2" is more energy efficient than 8PSK, as it advantageously uses constant envelop power amplifiers [47, 48].

Figure 21 shows that "QPSK & SM4" outperforms all other "16QAM & Pattern p" schemes. As for the previous antenna, "QPSK & SM4" is also more energy efficient than 16QAM, as it uses constant envelop amplifiers. Therefore, there is still room for improvement of the compactness of the antenna before the same BER vs SNR performance as 16QAM is attained.

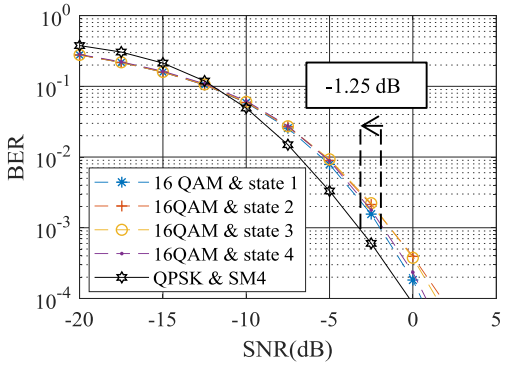

FIGURE 21. Performance with the multiport antenna.

Based on these current results, as illustrated in Figure 22, one path for future improvements is to build a new monoport reconfigurable antenna, that is more compact than the current multiport antenna, and to deliver 4 bits/s/Hz with a constant envelop modulation (the same "QPSK & SM4" scheme for instance).

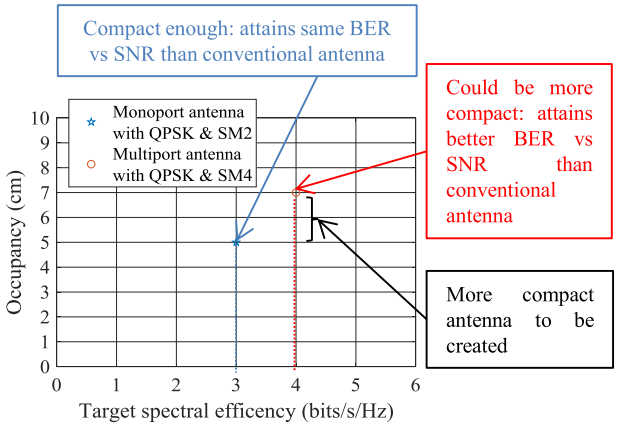

FIGURE 22. Path for improvement of the antenna for 4 bits/s/Hz.

V. DOWNLINK TRANSMISSION: FIRST PERFORMANCE EVALUATION OF TRANSMIT SPATIAL MODULATION WITH REAL COMPACT ANTENNAS

In this section, for the first time, we present a complete performance evaluation of a wireless communication system using receive spatial modulation with a real and existing compact antenna at the object side and an M-MIMO antenna at the network side. The considered carrier frequency in this section is 2.43 GHz.

A. REAL COMPACT MULTIPORT ANTENNA

At the base station side, we consider a ULA of $M = 64$ elements spaced by half a wavelength as an example of M-MIMO antenna.

The same real and existing compact multiport antenna [42] as the one used in Section III, and illustrated in Figure 12 is used. However, this time, there is no switch, and all the ports are used simultaneously. A similar 2D channel model as the one used in section III-A is used. This time, we define $\mathbf{H} \in \mathbb{C}^{P\times M}$ as the channel from the base station to the object, including wireless propagation and antenna radiation patterns. More precisely, let $\mathbf{H}_{p,m}$ be the channel coefficient between the transmit antenna $m \in [1, M]$ of the base station and the antenna port $p \in [1, 4]$ of the object. $\mathbf{H}_{p,m}$ includes both the wireless propagation and the radiation pattern of the port p.

As in Section III-A and as illustrated in Figure 23, we consider a 2D wireless multipath propagation model, with R random scatterers creating angular diversity in the channel. The antenna elements of the M-MIMO are spatially correlated. The path number $q \in [1, Q]$ between the transmit antenna m of the base station and the connected object has a random complex path gain $\Gamma_q \in \mathbb{C}$, a random angle of departure $\theta_q^{\mathrm{AoD}} \in [0, 2\pi]$ and a random angle of arrival $\theta_q^{\mathrm{AoA}} \in [0, 2\pi]$. Γ_q is Rayleigh distributed with $E\left[\left|\Gamma_q\right|^2\right] = 1/\mathrm{Q}$ and θ_q^{AoD} and θ_q^{AoA} are uniformly distributed over $[0,2\pi]$. With this notation, the channel coefficient $\mathbf{H}_{p,m}$ is given by:

$$\mathbf{H}_{p,m} = \rho \sum_{q=1}^{Q} \Gamma_q \delta_p\left(\theta_q^{\mathrm{AoA}}\right) e^{j\pi.sin\left(\theta_q^{\mathrm{AoD}}\right)(m-1)}, \quad (2)$$

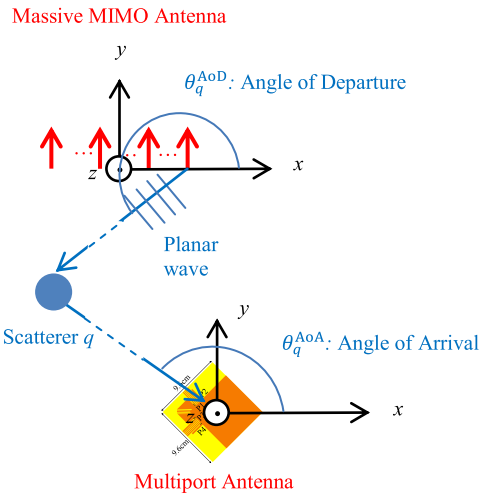

FIGURE 23. Propagation model for the multiport antenna.

where ρ is a normalizing factor. We choose ρ such that:

$$\frac{\|\mathbf{H}\|^2}{PM} = 1.$$

The average channel power per single antenna link is unitary.

B. SYSTEM MODEL

We compare the following five different schemes:

- "16QAM & Pattern $p = 1$";
- "16QAM & Pattern $p = 2$";
- "16QAM & Pattern $p = 3$";
- "16QAM & Pattern $p = 4$";
- "QPSK & SM4".

For all schemes, for each symbol period, the base station sends a sequence of 4 bits $\mathbf{b} = \mathbf{b}_1\mathbf{b}_2\mathbf{b}_3\mathbf{b}_4 \in \mathcal{B}^{(16)}$ using a complex modulation symbol s and a precoder $\mathbf{\Gamma}^{(p)}$, with $p \in [1, 4]$, picked among 4 stored precoders. The precoder $\mathbf{\Gamma}^{(p)} \in \mathbb{C}^{M\times P}$ is based on the MRT precoder and is defined as follows:

$$\mathbf{\Gamma}^{(p)}_{m,p} = \alpha^{(p)} \left(\mathbf{H}_{p,m}\right)^*, \tag{3}$$

where, $\alpha^{(p)}$ is chosen so that:

$$\sum\nolimits_{m=1}^{M} \left|\mathbf{\Gamma}^{(p)}_{m,p}\right|^2 = 1.$$

We denote by S the set of complex modulation symbols. The definition of S and the choice of p are scheme-specific and provided hereafter for each scheme.

In "16QAM & Pattern p", the precoder $\mathbf{\Gamma}^{(p)}$ is fixed, and 16QAM modulation is used, hence:

$$S = S^{\text{16QAM}}.$$

The pattern-to-bit mapping in Table 3 is used.

In the "QPSK & SM4" scheme, as illustrated in Figure 24, during each symbol period, $\mathbf{b}_1\mathbf{b}_2$ is sent using QPSK modulation. Simultaneously, $\mathbf{b}_3\mathbf{b}_4$ is sent using the corresponding precoder $\mathbf{\Gamma}^{(p)}$ (using the pattern-to-bit mapping rule of Table 3), hence:

$$S = S^{\text{QPSK}}.$$

The illustration of the mapping between bits and symbols in Figure 18 and the spectral efficiency given in Table 3 is still valid for the considered scheme. Note that with the chosen definitions, $E\left[|s|^2\right] = 1$ for all schemes. In other terms, all schemes require the same transmit power per symbol, in average.

We use the same notation X as for section III:

$$X = \{\mathbf{x}^{(l)} \in \{0, 1\}^{K\times 1} | 1 \le l \le 4, \mathbf{x}^{(l)}_l = 1 \,\&\, \mathbf{x}^{(l)}_{p\neq l} = 0.$$

Let $\mathbf{y} \in C^{M\times 1}$ be the signal received over the $P = 4$ ports of the object. With this notation, we obtain the following expression of $\mathbf{y}$:

$$\mathbf{y} = \mathbf{H}\mathbf{\Gamma}^{(p)}\mathbf{x}s\sqrt{P_u} + \boldsymbol{\nu},$$

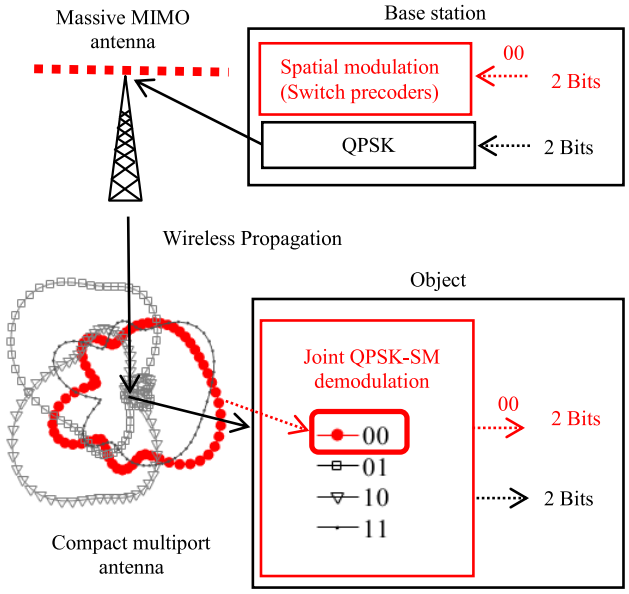

FIGURE 24. "QPSK & SM4" system model.

where $\mathbf{x} \in X$, $s \in S$, P_{U} is the transmit power and $\boldsymbol{\nu} \in \mathbb{C}^{M\times 1}$ is the vector of noise samples over the P ports of the object. We denote $P_{\text{NOISE}} = E\left[\|\boldsymbol{\nu}\|^2\right]/P$, as the average receiver noise power at the object side per port. We define an arbitrary signal to noise ratio metric *SNR* that is at least common to all schemes, as follows:

$$SNR = \frac{P_{\text{U}}}{P_{\text{NOISE}}}.$$

We assume that the receiver has perfect estimates of $\mathbf{H}$ and $\mathbf{\Gamma}^{(p)}$ thanks to a previous training phase based on pilots. We assume that the receiver has computed and stored the variables:

$$Y^{ref} = \left\{y = \mathbf{\Gamma}^{(p)}\mathbf{H}\mathbf{x}^{(p)}s\sqrt{P_u} | p \in [1, 4] \& s \in S\right\}.$$

Upon the reception of a new signal $\mathbf{y}$, the receiver compares it to the set of variables Y^{ref} and determines the signal $\hat{\mathbf{y}}$ that minimizes the Mean Square Error:

$$\hat{\mathbf{y}} = \left\{\frac{\|z - y\|^2}{M} | z \in Y^{ref}\right\}.$$

Then, the detected binary sequence $\hat{\mathbf{b}} = \hat{\mathbf{b}}_1\hat{\mathbf{b}}_2\hat{\mathbf{b}}_3\hat{\mathbf{b}}_4$ is deduced from $\hat{\mathbf{y}}$ by using the mapping rule illustrated in Figure 18.

We perform a large number of simulation runs (100,000 runs) and use the same simulation methodology as in Section IV-B) to derive the average the BER versus *SNR* curves of Figure 25.

C. SIMULATION RESULTS

Figure 25 shows that "16QAM & SM4" outperforms all other schemes for the considered range of SNR and BER values. This is due to the combination of two effects. On the one hand, "16QAM & SM4" is less dense in the complex domain

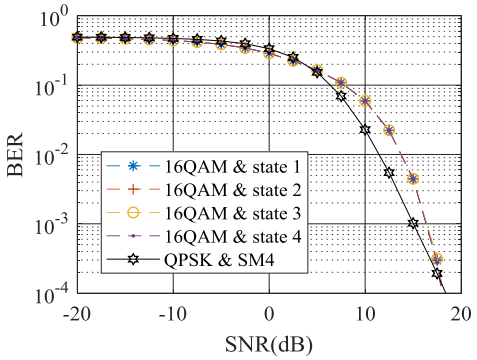

FIGURE 25. Simulation results.

than the "16QAM & Pattern p" modulations, as illustrated in Figure 18. On the other hand, the patterns of the 4-Port compact antenna are low correlated, as shown by Table 1.

We also observe that the BER performance of "QPSK & SM4" will be worse than that of 16 QAM modulation for higher SNR values. This is consistent with earlier studies on spatial modulation with conventional antenna arrays, led by at least two different independent teams in [49] (Fig. 5, Fig. 6 and Fig. 9) and in [50] (Fig. 9). These studies show that spatial modulation is outperformed by conventional modulations at high SNR.

To summarize the results, "QPSK & SM4" is a new modulation which, compared to 16QAM, is more energy efficient, in the considered ranges of SNR and BER values (larger than 10^{-4}).

VI. CONCLUSIONS AND FUTURE PERSPECTIVES

In this paper, for the first time, we have presented a complete performance evaluation results of two new wireless communication systems for small connected objects, both based on spatial modulation and real existing compact antennas at the object side, and M-MIMO antennas at the base station side. Based on experimental results, we have shown that introducing M-MIMO in 5G networks enables the potential re-introduction of single-carrier modulation based on spatial modulation. Our simulations take into account precise models of several real and existing compact antennas (obtained from actual prototypes designed and implemented for special application to single-carrier spatial modulation systems) at the object side: a compact monoport reconfigurable antenna with two states and a multiport switchable antenna with four states. We have compared the proposed spatial modulation systems with conventional modulations of the same spectral efficiency. Our results show that transmit spatial modulation with the monoport antenna attains the same BER versus SNR performance as 8PSK, but it allows one to use constant envelop amplifiers, which are less complex and more energy efficient. Transmit spatial modulation with the multiport antenna attains a better BER versus SNR than 16QAM, and still with constant envelop power amplifiers. For this higher spectral efficiency, a more compact antenna could still be designed. Our simulations also show that receive spatial modulation with the multiport antenna outperforms 16QAM. Future investigations will focus on the design of antennas providing optimum performance and compactness, for a given target spectral efficiency.

REFERENCES

[1] A. Ijaz *et al.*, "Enabling massive IoT in 5G and beyond systems: PHY radio frame design considerations," *IEEE Access*, vol. 4, pp. 3322–3339, 2016.
[2] *Technical Report 3rd Generation Partnership Project; Technical Specification Group GSM/EDGE Radio Access Network; Cellular System Support for Ultra-Low Complexity and Low Throughput Internet of Things (CIoT) (Release 13)*, document 3GPP TR 45.820 V13.1.0, Nov. 2015.
[3] R. Y. Mesleh, H. Haas, S. Sinanovic, C. W. Ahn, and S. Yun, "Spatial modulation," *IEEE Trans. Veh. Technol.*, vol. 57, no. 4, pp. 2228–2241, Jul. 2008.
[4] M. Di Renzo, H. Haas, and P. M. Grant, "Spatial modulation for multiple-antenna wireless systems: A survey," *IEEE Commun. Mag.*, vol. 49, no. 12, pp. 182–191, Dec. 2011.
[5] A. Stavridis, S. Sinanovic, M. Di Renzo, and H. Haas, "Energy evaluation of spatial modulation at a multi-antenna base station," in *Proc. IEEE 78th Veh. Technol. Conf. (VTC Fall)*, Las Vegas, NV, USA, Sep. 2013, pp. 1–5.
[6] M. Di Renzo and H. Haas, "On transmit diversity for spatial modulation MIMO: Impact of spatial constellation diagram and shaping filters at the transmitter," *IEEE Trans. Veh. Technol.*, vol. 62, no. 6, pp. 2507–2531, Jul. 2013.
[7] A. Younis *et al.*, "Performance of spatial modulation using measured real-world channels," in *Proc. IEEE 78th Veh. Technol. Conf. (VTC Fall)*, Las Vegas, NV, USA, Sep. 2013, pp. 1–5.
[8] N. Serafimovski *et al.*, "Practical implementation of spatial modulation," *IEEE Trans. Veh. Technol.*, vol. 62, no. 9, pp. 4511–4523, Nov. 2013.
[9] J. Zhang, Y. Wang, L. Ding, and N. Zhang, "Bit error probability of spatial modulation over measured indoor channels," *IEEE Trans. Wireless Commun.*, vol. 13, no. 3, pp. 1380–1387, Mar. 2014.
[10] S. Gokceli, E. Basar, M. Wen, and G. K. Kurt, "Practical implementation of index modulation-based waveforms," *IEEE Access*, vol. 5, pp. 25463–25473, 2017.
[11] E. Soujeri and G. Kaddoum, "The impact of antenna switching time on spatial modulation," *IEEE Wireless Commun. Lett.*, vol. 5, no. 3, pp. 256–259, Jun. 2016.
[12] R. Mesleh, O. Hiari, A. Younis, and S. Alouneh, "Transmitter design and hardware considerations for different space modulation techniques," *IEEE Trans. Wireless Commun.*, vol. 16, no. 11, pp. 7512–7522, Nov. 2017.
[13] O. Hiari and R. Mesleh, "A reconfigurable SDR transmitter platform architecture for space modulation MIMO techniques," *IEEE Access*, vol. 5, pp. 24214–24228, 2017.
[14] J. Verhaevert and P. Van Torre, "Realization and MIMO-link measurements of a transmit module for spatial modulation," in *Proc. 9th Eur. Conf. Antennas Propag. (EuCAP)*, Lisbon, Portugal, 2015, pp. 1–5.
[15] L. Xiao *et al.*, "Time-domain turbo equalization for single-carrier generalized spatial modulation," *IEEE Trans. Wireless Commun.*, vol. 16, no. 9, pp. 5702–5716, Sep. 2017.
[16] L. Xiao, L. Dan, Y. Zhang, Y. Xiao, P. Yang, and S. Li, "A low-complexity detection scheme for generalized spatial modulation aided single carrier systems," *IEEE Commun. Lett.*, vol. 19, no. 6, pp. 1069–1072, Jun. 2015.
[17] L. Xiao, P. Yang, Y. Zhao, Y. Xiao, J. Liu, and S. Li, "Low-complexity tree search-based detection algorithms for generalized spatial modulation aided single carrier systems," in *Proc. IEEE Int. Conf. Commun. (ICC)*, Kuala Lumpur, Malaysia, May 2016, pp. 1–6.
[18] M. Di Renzo, H. Haas, A. Ghrayeb, S. Sugiura, and L. Hanzo, "Spatial modulation for generalized MIMO: Challenges, opportunities, and implementation," *Proc. IEEE*, vol. 102, no. 1, pp. 56–103, Jan. 2014.
[19] P. Yang, M. Di Renzo, Y. Xiao, S. Li, and L. Hanzo, "Design guidelines for spatial modulation," *IEEE Commun. Surveys Tuts.*, vol. 17, no. 1, pp. 6–26, 1st Quart., 2015.
[20] P. Yang *et al.*, "Single-carrier SM-MIMO: A promising design for broadband large-scale antenna systems," *IEEE Commun. Surveys Tuts.*, vol. 18, no. 3, pp. 1687–1716, 3rd Quart., 2016.
[21] E. Basar, M. Wen, R. Mesleh, M. Di Renzo, Y. Xiao, and H. Haas, "Index modulation techniques for next-generation wireless networks," *IEEE Access*, vol. 5, pp. 16693–16746, 2017.

[22] P. Liu, J. Blumenstein, N. S. Perović, M. Di Renzo, and A. Springer, "Performance of generalized spatial modulation MIMO over measured 60 GHz indoor channels," *IEEE Trans. Commun.*, vol. 66, no. 1, pp. 133–148, Jan. 2018.
[23] E. Basar. (Nov. 2018). "Media-based modulation for future wireless systems: A tutorial." [Online]. Available: https://arxiv.org/abs/1811.08730
[24] E. Basar and I. Altunbas, "Space-time channel modulation," *IEEE Trans. Veh. Technol.*, vol. 66, no. 8, pp. 7609–7614, Aug. 2017.
[25] I. Yıldırım, E. Basar, and I. Altunbas, "Quadrature channel modulation," *IEEE Wireless Commun. Lett.*, vol. 6, no. 6, pp. 790–793, Dec. 2017.
[26] D. T. Phan-Huy and M. Hélard, "Receive antenna shift keying for time reversal wireless communications," in *Proc. IEEE Int. Conf. Commun. (ICC)*, Jun. 2012, pp. 4852–4856.
[27] A. Mokh, M. Crussière, and M. Hélard, "Performance analysis of the maximum ratio transmission preprocessing for extended receive antenna shift keying," in *Proc. 20th Int. Symp. Wireless Pers. Multimedia Commun. (WPMC)*, Bali, Indonesia, 2017, pp. 271–275.
[28] A. Mokh, M. Hélard, and M. Crussière, "Space shift keying modulations for low complexity Internet-of-Things devices," in *Proc. IEEE Global Commun. Conf. (GLOBECOM)*, Singapore, Dec. 2017, pp. 1–7.
[29] A. Mokh, Y. Kokar, M. Hélard, and M. Crussière, "Time reversal receive antenna shift keying on MIMO LOS channel," in *Proc. Sensors Netw. Smart Emerg. Technol. (SENSET)*, Beirut, Lebanon, 2017, pp. 1–4.
[30] O. N. Alrabadi, J. Perruisseau-Carrier, and A. Kalis, "MIMO transmission using a single RF source: Theory and antenna design," *IEEE Trans. Antennas Propag.*, vol. 60, no. 2, pp. 654–664, Feb. 2012.
[31] M. A. Sedaghat, R. R. Mueller, G. Fischer, and A. Ali, "Discrete load-modulated single-RF MIMO transmitters," in *Proc. 20th Int. ITG Workshop Smart Antennas (WSA)*, Munich, Germany, 2016, pp. 1–7.
[32] M. Di Renzo, "Spatial modulation based on reconfigurable antennas—A new air interface for the IoT," in *Proc. MILCOM*, Oct. 2017, pp. 495–500.
[33] H. Yu, G. Yang, F. Meng, and Y. Li, "Performance analysis of MIMO system with single RF link based on switched parasitic antenna," *Basel*, vol. 9, no. 12, p. 304, 2017.
[34] H. Yang and T. L. Marzetta, "Performance of conjugate and zero-forcing beamforming in large-scale antenna systems," *IEEE J. Sel. Areas Commun.*, vol. 31, no. 2, pp. 172–179, Feb. 2013.
[35] V. Jungnickel *et al.*, "The role of small cells, coordinated multipoint, and massive MIMO in 5G," *IEEE Commun. Mag.*, vol. 52, no. 5, pp. 44–51, May 2014.
[36] T. Dubois, M. Hélard, M. Crussière, and I. Maaz, "Time reversal applied to large MISO-OFDM systems," in *Proc. IEEE 24th Annu. Int. Symp. Pers., Indoor, Mobile Radio Commun. (PIMRC)*, London, U.K., Sep. 2013, pp. 896–901.
[37] P. Pajusco, F. Gallée, N. Malhouroux, and R. Burghelea, "Massive antenna array for space-time channel sounding," in *Proc. 11th Eur. Conf. Antennas Propag. (EUCAP)*, Paris, France, 2017, pp. 865–868.
[38] *IEEE ICC 2017 Spatial Modulation Demonstration*. [Online]. Available: https://www.youtube.com/watch?v=L7xAeU2jh5s
[39] Y. Kokar, J.-C. Prévotet, and M. Hélard, "Receive antenna shift keying modulation testbed for wireless communications systems," in *Proc. IEEE Globecom*, Washington, DC, USA, Dec. 2016, pp. 1–6.
[40] T. K. Y. Lo, "Maximum ratio transmission," *IEEE Trans. Commun.*, vol. 47, no. 10, pp. 1458–1461, Oct. 1999.
[41] G. Lerosey, C. Leray, F. Lemoult, J. de Rosny, A. Tourin, and M. Fink, "Hybridization band gap based smart antennas: Deep subwavelength yet directional and strongly decoupled MIMO antennas," in *Proc. 6th Eur. Conf. Antennas Propag. (EUCAP)*, Prague, Czech Republic, 2012, pp. 2697–2701.
[42] N. M. Gaffet, P. Pajusco, R. Burghelea, and C. Leray, "Capacity gain of MIMO systems with micro-structured antenna arrays," in *Proc. Eur. Conf. Antennas Propag. (EUCAP)*, The Hague, The Netherlands, 2014, pp. 2551–2555.
[43] D.-T. Phan-Huy, T. Sarrebourse, A. Gati, J. Wiart, and M. Hélard, "Characterization of the confidentiality of a green time reversal communication system: Experimental measurement of the spy BER sink," in *Proc. IEEE Wireless Commun. Netw. Conf. (WCNC)*, Shanghai, China, Apr. 2013, pp. 4783–4788.
[44] D. T. Phan-Huy, S. Ben Halima, and M. Hélard, "Dumb-to-perfect receiver throughput ratio maps of a time reversal wireless indoor system," in *Proc. ICT*, Casablanca, Morocco, 2013, pp. 1–5.
[45] *Open Air Interface*. [Online]. Available: www.openairinterface.org/
[46] A. Ourir, K. Rachedi, D.-T. Phan-Huy, C. Leray, and J. de Rosny, "Compact reconfigurable antenna with radiation pattern diversity for spatial modulation," in *Proc. EuCAP*, 2017, pp. 3038–3043.
[47] J. Joung, C. K. Ho, K. Adachi, and S. Sun, "A survey on power-amplifier-centric techniques for spectrum- and energy-efficient wireless communications," *IEEE Commun. Surveys Tuts.*, vol. 17, no. 1, pp. 315–333, 1st Quart., 2015.
[48] P. E. Chadwick *et al.*, *Constant Envelop Modulation, IEEE 802.11 Wireless Access Method And Physical Specification*, document IEEE P802.11-93/80, May 1993. [Online]. Available: http://www.ieee802.org/11/Documents/DocumentArchives/1993_docs/1193080_scan.pdf
[49] J. Jeganathan, A. Ghrayeb, L. Szczecinski, and A. Ceron, "Space shift keying modulation for MIMO channels," *IEEE Trans. Wireless Commun.*, vol. 8, no. 7, pp. 3692–3703, Jul. 2009.
[50] M. Di Renzo and H. Haas, "Bit error probability of SM-MIMO over generalized fading channels," *IEEE Trans. Veh. Technol.*, vol. 61, no. 3, pp. 1124–1144, Mar. 2012.

D.-T. PHAN-HUY received the degree in engineering from Supelec, in 2001, and the Ph.D. degree in electronics and telecommunications from the National Institute of Applied Sciences of Rennes, France, in 2015. In 2001, she joined France Telecom R&D (now Orange Labs Networks), Châtillon, France. She received the "Prix Impact Economique des Rencontres du Numérique 2016." She leads the SpatialModulation Project. Her research interests include wireless communications and beamforming.

Y. KOKAR received the master's degree in engineering from the Graduate Engineering School, Montpellier University, Montpellier, France, in 2004. In 2006, he joined the Electronics and Telecommunications Institute of Rennes Laboratory, Institut d'Electronique et de Télécommunication de Rennes, as a Research Engineer. His research interests include the intersection of communication theory, wireless networks, and their implementation through hardware and software defined.

K. RACHEDI received the License degree in electronics and the master's degree of RF and electromagnetism from University Pierre and Marie Curie, Paris, France, in 2014 and 2016, respectively. He is currently pursuing the Ph.D. thesis on reconfigurable antennas for spatial modulation communications with the Institut Langevin, Paris, France. His current research interest includes backscattering.

P. PAJUSCO (M'07–SM'13) received the degree in engineering from Supélec, in 1992, and the Ph.D. degree in electronics from the European University of Brittany, Rennes, France, in 2011. He joined CNET (now Orange Labs Networks), Belfort, France, in 1993. In 1999, he was in charge of the Channel Modeling Team. He joined the Institut Mines Telecom Atlantique, Brest, France, in 2008, where he is currently the Head of the Microwave Department. His research interests include wideband MIMO channel sounding and modeling.

A. MOKH was born in Al-Kwakh, Lebanon, in 1992. He received the Engineering degree in telecommunications from the Faculty of Engineering, Lebanese University, Lebanon, and the M.Sc. degree in signal processing from the Institut National Polytechnique de Grenoble, Phelma, France, in 2015. He is currently pursuing the Ph.D. degree with IETR, Institut d'Electronique et de Télécommunication de Rennes, France.

T. MAGOUNAKI graduated in electronic and computer engineering, telecommunications engineering from Polytechnion Kritis, Greece, in 2014, received the master's degree in mobile communications from Eurecom, Sophia Antipolis, France, in 2017. She is currently pursuing the Ph.D. degree with Orange Labs Networks, Sophia Antipolis. Her research interests include massive MIMO, time reversal, the Internet-of-Things, and open air interface.

R. MASOOD received the B.S. degree in electrical engineering from the University of Engineering and Technology, Lahore, Pakistan, in 2009, and the Ph.D. degree in communication engineering from Telecom Bretagne, Brest, France, in 2016, where he was a Postdoctoral Researcher till 2017. Since 2017, he has been a Research and Development Engineer with Orange Labs Networks, Rennes, France. His current research interests include radio channel and propagation, OFDM, LTE, and 5G.

C. BUEY received the B.S. degree in RF communication systems from Lille I University, in 2014, and the Ph.D. degree in electronic from Côte d'Azur University in collaboration with Orange Labs, Sophia Antipolis, in 2018. During his Ph.D., he worked on MIMO antenna designs and characterization. He developed innovative MIMO antennas for 4G femto-cell and Wi-Fi applications. He also developed a low-cost and open-source over-the-air measurement testbed for multi-antenna systems.

P. RATAJCZAK received the M.Sc. and Ph.D. degrees in electrical engineering from the Université of Nice-Sophia Antipolis, in 1990 and 1995, respectively. In 1995, he joined CNET (now Orange Labs), Sophia-Antipolis, France. Since 2014, he has been the Co-Head of the CREMANT, the antenna joint research center between Orange Labs Networks, the University of Nice and CNRS. He has co-authored more than 70 papers and 11 patents. His research interests include reflectarrays, reconfigurable antennas with beamforming capabilities, and electromagnetic modeling and simulation.

N. MALHOUROUX-GAFFET received the Ph.D. degree from Paris VI-VII University, in 1993, and the Ph.D. degree from the Laboratory of Electronic Philips, Department of Micro-Electronics, in collaboration with the CNRS, in 1992. In 1993, she joined France Telecom R&D (now Orange Labs Networks), Belfort, France. Her current research interests include massive MIMO systems and propagation characterization and modeling for 5G.

J.-M. CONRAT received the M.S. degree in electrical engineering from the National Institute of Applied Sciences, Lyon, France, in 1991. Since 1993, he has been with Orange Labs Netowrks, Belfort, France. He is involved in measurement equipment development and propagation channel measurements, modeling, and simulation. His current research interest includes the characterization of the directional wideband propagation channel for 5G millimeter wave systems.

J.-C. PRÉVOTET received the Ph.D. degree from UPMC, in 2003. He is currently an Associate Professor with IETR/ Institut d'Electronique et de Télécommunication de Rennes. His current interests include embedded and reconfigurable systems and real time systems in general. In particular, his applicative subjects deal with communication systems and the way to optimize their architecture onto real platform. He is also deeply involved in the real time management of these communication platforms under the supervision of an embedded operating system.

A. OURIR received the degree in engineering from ENIT, Tunis, Tunisia, in 2003, and the Ph.D. degree in physics from Paris Sud University, Orsay, France, in 2007. Since 2008, he has been a CNRS Research Engineer with the Institut Langevin, Paris, France. He is involved in SpatialModulation Project. He has developed original devices based on passive and active metamaterials for antennas. His current research interests include metamaterial based antennas, electromagnetic subwavelength imaging and wave propagation in artificial materials.

J. DE ROSNY received the M.S. and Ph.D. degrees in wave physics from University Pierre and Marie Curie, Paris, France, in 1996 and 2000, respectively. He held a Postdoctoral position with the Scripps Research Institute, CA, USA, from 2000 to 2001. In 2001, he joined with the Laboratoire Ondes et Acoustique, CNRS, France. Since 2014, he has been a CNRS Senior Scientist with the Institut Langevin, Paris, France. His research interests include telecommunications in complex media, acoustic, and electromagnetic waves-based imaging.

M. CRUSSIÈRE received the M.Sc. and Ph.D. degrees in electrical engineering from INSA Rennes, France, in 2002 and 2005, respectively. He then joined as an Associate Professor with the Institut d'Electronique et de Télécommunication de Rennes. He has co-authored about 110 technical papers in international conferences and journals. His current research interests include digital communications and signal processing, for adaptive multicarrier, multiantenna systems.

PR. M. HÉLARD received the engineering and Ph.D. degrees from the INSA of Rennes, France, in 1981 and 1884, respectively, and the Habilitation degree, in 2004. After being with Orange Labs as a Research Engineer, she joined the INSA Rennes as a Full Professor, in 2007, where she led the IETR Department. She was involved in several collaborative research projects. Her research interests include wired and wireless communications and MIMO techniques.

A. GATI received the Engineer degree in telecommunication and signal processing, in 1996, the M.Sc. degree from the University of Rennes, Rennes, France, and the Ph.D. degree from UPMC (Paris VI), Paris, France, in 2000. In 2001, he joined France Telecom R&D (now Orange Labs Networks), Châtillon, France. Since 2007, he has been leading research on sustainable development, including energy in information, communication technology, and service solutions.

T. SARREBOURSE was born in Nantes, France. He received the M.S. in sciences and technology of sciences from the University of Nantes. In 1990, he joined France Telecom R&D (now Orange Labs Networks), Châtillon, France. His research interests include electromagnetic fields measurements and simulations dealing with mobile communications and interactions with persons.

M. DI RENZO is currently a CNRS Associate Professor with the Laboratory of Signals and Systems, University of Paris-Saclay, Paris, France. He was a recipient of the IEEE Jack Neubauer Memorial Award, in 2015, the SEE-IEEE Alain Glavieux Award, in 2017, and among many other awards. He is an Associate Editor-in-Chief of the IEEE COMMUNICATIONS LETTERS, an Editor of the IEEE TRANSACTIONS ON COMMUNICATIONS and the IEEE TRANSACTIONS ON WIRELESS COMMUNICATIONS.